A satellite snow depth multi-year average derived from SSM/I for the high latitude regions

Sylvain Biancamaria [a,*], Nelly M. Mognard [a], Aaron Boone [b],
Manuela Grippa [c], Edward G. Josberger [d]

[a] Laboratoire d'Etudes en Géophysique et Océanographie Spatiales (LEGOS), CNES/CNRS/IRD/UPS, 14 Av. E. Belin, 31400 Toulouse, France
[b] GAME/CNRM, Météo-France, CNRS, 42 Av. G. Coriolis, 31057 Toulouse Cedex, France
[c] Centre d'Etudes Spatiales de la BIOsphère (CESBIO), CNES/CNRS/IRD/UPS, 18 Av. E. Belin, 31400 Toulouse, France
[d] United States Geological Survey (USGS), 934 Broadway, Tacoma, WA 98042, USA

Abstract

The hydrological cycle for high latitude regions is inherently linked with the seasonal snowpack. Thus, accurately monitoring the snow depth and the associated aerial coverage are critical issues for monitoring the global climate system. Passive microwave satellite measurements provide an optimal means to monitor the snowpack over the arctic region. While the temporal evolution of snow extent can be observed globally from microwave radiometers, the determination of the corresponding snow depth is more difficult. A dynamic algorithm that accounts for the dependence of the microwave scattering on the snow grain size has been developed to estimate snow depth from Special Sensor Microwave/ Imager (SSM/I) brightness temperatures and was validated over the U.S. Great Plains and Western Siberia.

The purpose of this study is to assess the dynamic algorithm performance over the entire high latitude (land) region by computing a snow depth multi-year field for the time period 1987–1995. This multi-year average is compared to the Global Soil Wetness Project-Phase2 (GSWP2) snow depth computed from several state-of-the-art land surface schemes and averaged over the same time period. The multi-year average obtained by the dynamic algorithm is in good agreement with the GSWP2 snow depth field (the correlation coefficient for January is 0.55). The static algorithm, which assumes a constant snow grain size in space and time does not correlate with the GSWP2 snow depth field (the correlation coefficient with GSWP2 data for January is −0.03), but exhibits a very high anti-correlation with the NCEP average January air temperature field (correlation coefficient −0.77), the deepest satellite snow pack being located in the coldest regions, where the snow grain size may be significantly larger than the average value used in the static algorithm. The dynamic algorithm performs better over Eurasia (with a correlation coefficient with GSWP2 snow depth equal to 0.65) than over North America (where the correlation coefficient decreases to 0.29).
© 2007 Elsevier Inc. All rights reserved.

Keywords: SSM/I; GSWP2; Snow depth; High latitude regions; Tundra; Taiga; Lakes

1. Introduction

Several studies have shown the importance of taking into account the large spatial scale snowpack evolution in order to better understand arctic river discharge regimes (Cao et al., 2002; Rango, 1997; Rawlins et al., 2006). As these rivers supply fresh water to the Arctic Ocean, a modification in their discharge, induced by a change in snow fall, could lead to a modification in the thermohaline circulation. Moreover, the snowpack is an important component of the climate system and its depletion may increase global warming through feedback processes (Hall, 2004). Therefore, the monitoring of the snow depth and its extent is a key issue to understand the hydrological cycle and its relation to climate change at high latitudes.

Over high latitude regions, in-situ measurements are very sparse and do not allow the accurate estimation of the global snowpack. Passive microwave satellite sensors are well suited for this purpose as they are sensitive to both snow extent and snow depth. Yet, snow depth retrieval from SSM/I brightness temperature is difficult because snow emissivity is also sensitive to the snow grain size (Tsang et al., 2000) which is highly

---

variable and depends on the bulk temperature gradient through the snowpack (Sturm and Benson, 1997). In order to take into account the variability of the snow grain size, a snow depth dynamic retrieval algorithm has been developed and validated over the Northern Great Plains (Josberger and Mognard, 2002; Mognard and Josberger, 2002) and over West Siberia (Boone et al., 2006; Grippa et al., 2004, 2005a).

The main objective of this study is to validate the dynamic algorithm over the entire high latitude regions, by comparing the satellite snow depth multi-year average from 1987 to 1995 to the snow depth multi-year average over the same time period from a land surface scheme (LSS) reanalysis product obtained from the Global Soil Wetness Project Phase 2 (GSWP2). GSWP2 drives several state-of-the-art LSS using the best quality atmospheric and land surface databases, and long-term monitoring sites to produce global land surface fluxes and state variables (Dirmeyer et al., 2006), such as snow depth (SD) and snow water equivalent (SWE). Hence, it is analogous to the NCEP atmospheric reanalysis program. For this snow study, the SD obtained from the static retrieval algorithm developed by Chang et al. (1987) (which assumes a spatially and temporally constant snow grain size) is compared to the SD from the dynamic algorithm.

2. Study area and datasets

This section describes the input satellite data used by the snow depth retrieval algorithms, the ancillary input data, the snow depth multi-year average used to validate the satellite retrieval algorithms and the main study area characteristics. The vegetation and lake classifications used for a more detailed validation are also presented herein. The time period of this study extends from October 1987 to September 1995, which is the common time period for both SSM/I and GSWP2 datasets.

2.1. Study area

The study area corresponds to the high latitude regions with latitudes higher than 50° North. Fig. 1a shows a topographic map of this region. The main vegetation zones consist of steppe and agricultural areas at lower latitudes, taiga and tundra at higher latitudes (Fig. 1b). In addition, there are a large number of lakes in the study domain, especially in North America (Fig. 1c), which provides an additional factor of diversity in the surface emissivities.

2.2. SSM/I data

The Special Sensor Microwave/Imager (SSM/I) measures the earth emissivity in seven microwave frequencies with horizontally and vertically polarized channels at 19.35, 37 and 85.5 GHz and a vertically polarized channel at 22.235 GHz. Since July, 1987, this instrument has been operating on board the operational Defense Meteorological Satellite Program satellite series (DMSP F-8, F-11 and F-13 platforms). For these frequencies Chang et al. (1987), showed that the 37 GHz channel is the channel suitable to study the snowpack when

combined with the 19 GHz channel, which reduces the effects of ground temperature and atmospheric perturbations on changes in brightness temperatures. Both the static and the
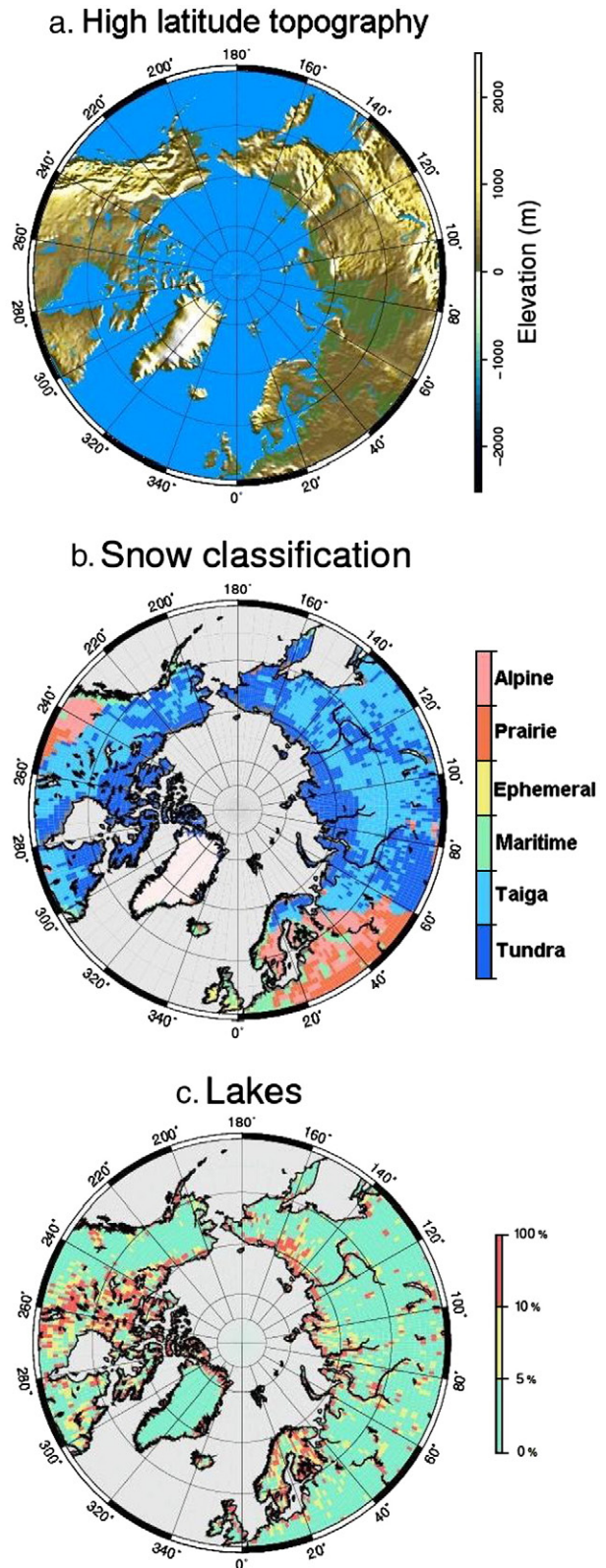

Fig. 1. Maps of different parameters characterizing the high latitude regions: topography from NGDC 5 min Digital Elevation Model (a), snow classification from Liston and Sturm (1998) (b) and percentage of lakes from IGBP (c).

dynamic algorithms employ the spectral gradient, which is defined here as the difference between the horizontally polarized 19 and 37 GHz channels.

Daily SSM/I data have been provided by the National Snow and Ice Data Center (NSIDC), mapped to the Equal Area SSM/I Earth Grid (EASE-Grid) with a 25×25 km^2 resolution (Armstrong et al., 1994). To minimize the spatial gaps resulting from the swath width, the daily data were averaged over pentads (5-days periods).

2.3. Ancillary input data for the dynamic algorithm

For cold snowpacks, the snow grain size growth is primarily driven by the temperature gradient through the snowpack. In the dynamic algorithm, this gradient represents the difference between the atmosphere/snow interface (referred to herein as "air") and the ground/snow interface temperatures. For the air temperature, the National Center for Environmental Prediction (NCEP) global reanalysis has been used, available from the Joint Institute for the Study of Atmosphere and Ocean (JISAO) (Kalnay et al., 1996). The NCEP air temperatures have been interpolated to the EASE-Grid and averaged into pentads.

To estimate the temperature at the base of the snowpack, the ground temperature simulated by the Interaction between the Soil–Biosphere–Atmosphere (ISBA) LSS is used. ISBA (Noilhan and Mahfouf, 1996) is a state-of-the-art LSS which has been developed at Météo-France. Boone et al. (2006) explain in details how ISBA has been run to obtain the soil temperature. Briefly, ISBA has been used with the explicit soil diffusion option (Boone et al., 2000) with a six-layer soil configuration with the highest vertical resolution at the surface. The uppermost soil temperature (centred at 0.015 m) is assumed to represent the temperature at the soil-snow interface (at $z = 0$). This approximation has negligible impact, especially since monthly averages are used in this study. ISBA was forced with the GSWP2 database to produce the averaged pentad ground temperatures for a 13 years period (1982–1994) mapped into EASE-grid.

2.4. Evaluation data

The datasets used to validate or investigate the spatial behaviour of the retrieval algorithms, namely the GSWP2 snow depth and the land cover classification, are presented in this section.

2.4.1. GSWP2 snow depth

A crucial issue for remote sensing based algorithms is validation, particularly over the high latitude regions, where in situ observations are extremely sparse. Grippa et al. (2004) emphasized the difficulty in comparing local scale data to large scale averages. Indeed, point observations are of limited value when looking at data over the relatively large spatial scales considered herein. Chang et al. (2005) performed a geostatistical analysis of snow gauge data in the Northern Great Plains of the USA and estimated the snow depth error to be about 22 cm for one station on a $1° \times 1°$ grid cell. For this reason the retrieval

algorithm performance has been evaluated by comparing to the global model-based analysis snow depth product from the GSWP2 rather than to snow gauge data.

For this study, the GSWP2 snow depth fields represent an average of the snow depth output from five LSS: MOSES (from the U. K. Met. Office, Exeter, UK), NOAH (National Center for Environmental Prediction, Camp Springs, USA), NSIPP (NASA Goddard, Greenbelt, USA), SSiB (Center for Ocean Land Atmosphere studies, Calverton, USA) and SWAP (Institute of Water Problems, Moscow, Russia). This averaging was performed to reduce the influence of single LSS, which can be large at high latitudes (Schlosser et al., 2000). The input atmospheric forcing database used to drive the LSS is the NCEP-DOE reanalysis (Kanamitsu et al., 2002), which has been "hybridized" (corrected using observed and satellite based precipitation data). These five LSS have been run for the period from 1986 to 1995 and a monthly multi-year average for the same period as the SSM/I data (October 1987 to September 1995) has been derived with a spatial resolution of $1° \times 1°$. Fig. 2a presents the average GSWP2 January snow depth. To quantify the spread amongst the 5 LSS, the inter-model coefficient of variation (CV) was computed (quotient of the standard deviation of the 5 LSS by their mean). Fig. 2b shows that globally, for the regions with large snow depth (SD>30 cm), the scatter is low (CV ~ 20%) while for regions with lower SD, the CV increases to 40%, especially east of the Lena river The inter-model spread is globally low and the averaging (Fig. 2a) minimizes individual model biases.

Fig. 2c shows the USAF/ETAC snow depth climatology for January (Foster and Davy, 1988) which approximately represents a mean on a 30 year period ending in the 1980s. The manually edited snow depths were derived from many sources based on an extensive literature search. Fig. 2d shows the corresponding NCEP air January temperature field. Globally, the snow accumulation areas are the same for ETAC and GSWP2, except around 160°E, where ETAC shows a local maximum that is not present in GSWP2. The correlation coefficient between ETAC and GSWP2 is 0.53, the differences come from errors in snow depth field from GSWP2 (input errors, models errors, …), errors in the ETAC climatology (few in-situ data, interpolation method, …) and also from the differences in the time period considered in regions that have the strongest response to climate warming. The characteristic features of these snow depth fields are similar, even if GSWP2 snow depths are greater than ETAC. Even if this analysis cannot quantitatively address the accuracy of the GSWP2 data, it is worthwhile to remember that the GSWP2 models are run with the best atmospheric reanalysis, which takes into account in-situ measurements. Thus, GSWP2 products are an equivalent of a reanalysis and provide the best possible estimate of land surface variables, like snow depth. Furthermore, they cover the same time period as SSM/I data, unlike the USAF/ETAC snow depth fields.

Similar results (relatively low inter-model scatter and the good agreement with in-situ based snow depth climatology) have been found for the other winter months. That is why GSWP2 snow depth fields have been used to validate the retrieval algorithms.
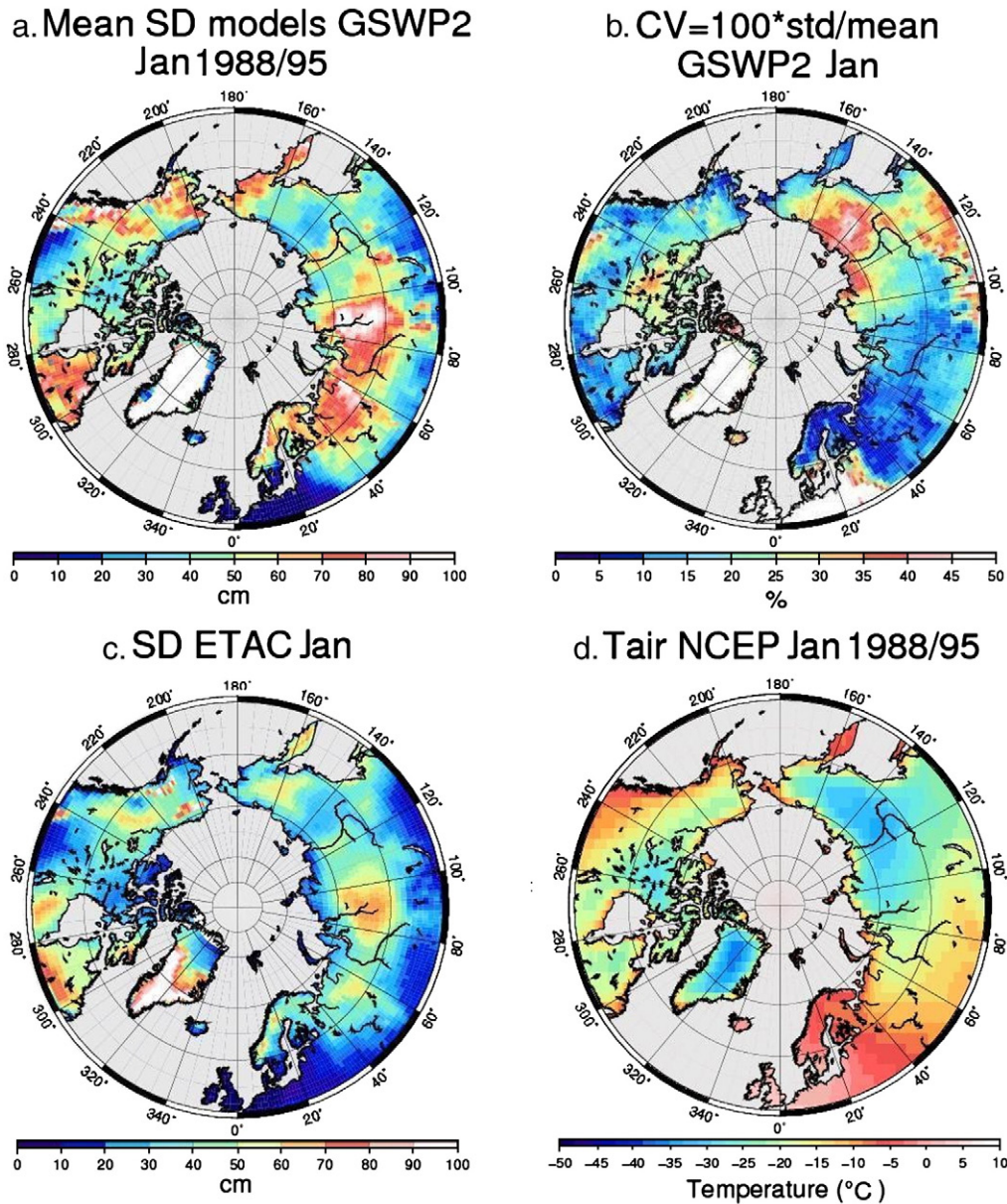
Fig. 2. GSWP2 snow depth inter-model mean in cm averaged from 1988 to 1995 (a), inter-model coefficient of variation (standard deviation/mean, b), snow depth mean from USAF/ETAC in cm (c) and NCEP air temperature in °C averaged from 1988 to 1995 (d), for January.

Since the GSWP2 models simulate the land surface state using a $1° \times 1°$ resolution, the snow depth over Alpine grid points represents values corresponding to an average elevation (mostly due to the spatially averaged air temperature). So, regions with high sub-grid ($1° \times 1°$) topographic variability will likely be the least reliable in terms of the snow product.

2.4.2. Land cover classification

Since vegetation cover affects brightness temperatures, the correlation between GSWP2 data and output from retrieval algorithms has been investigated over different vegetation areas. For the high latitude regions, the main vegetation classes are tundra and taiga. The classification used in this study is the snow classification from Sturm et al. (1995). The different classes, represented in Fig. 1b, are as follows: water, tundra

snow, taiga snow, maritime snow, ephemeral snow, prairie snow, alpine snow and ice, they have a spatial resolution of $0.5° \times 0.5°$ that has been resampled to a $1 \times 1°$ spatial resolution. Sturm et al. (1995) describes the tundra snow class as a thin, cold wind-blown snow area, usually found above or north of tree line, with a snow depth range from 10 to 75 cm and with a bulk density of 0.38 g cm^{-3}. The taiga snow class corresponds to a thin to moderately deep low-density cold snow cover found in cold climates in forests where wind, initial snow density, and average winter air temperatures are all low. The snow depth range from 30 to 120 cm and the bulk density is 0.26 g cm^{-3}. Over North America, tundra and taiga classes cover respectively 41% and 23% of the whole area, whereas over Eurasia tundra and taiga represent respectively 41% and 37% of the whole area.

To check the retrieval algorithms performance over areas with different percentages of lakes, data from the International Geosphere–Biosphere Program (IGBP) Earth surface classification (Belward et al., 1999) is used and mapped to the NSIDC EASE-Grid projection. The IGBP classification gives the percentage of lakes for each EASE-Grid pixel (Fig. 1c). The spatial distribution of lakes greatly differs between Eurasia and North America: according to IGBP, the areal extent covered with 10% of lakes or higher is much larger in North America than in Eurasia.

3. Methods

This section presents the algorithms used in the current study to retrieve snow depth from SSM/I data. The first algorithm (Section 3.1.) is a static algorithm developed by Chang et al. (1987), extensively used and referred to in the literature. The second algorithm is the dynamic algorithm described in Section 3.2. The third algorithm, presented in Section 3.3., is called the extended dynamic algorithm and computes the snow depth in regions where the dynamic algorithm cannot be applied due to the low temporal variations of the brightness temperature.

3.1. Static algorithm

The static algorithm developed by Chang et al. (1987), to retrieve snow depth from SSM/I data is given by the following equation:

$$SD = a \cdot SG = a \cdot (T_{b19H} - T_{b37H}) \quad (1)$$

where SD corresponds to the snow depth (in cm), $a = 1.59$ cm/K, SG is the spectral gradient and T_{bxH} is the SSM/I brightness temperature at a frequency of x GHz for horizontal polarization. The value of the a coefficient given above corresponds to a snow grain size (i.e. radius) of 0.3 mm. This algorithm has been widely used for the last two decades to retrieve snow depth at continental to hemispheric scales (Chang et al., 1990), for climate studies (Bamzai and Shukla, 1999; Wulder et al., 2007), global snow depth monitoring studies (Foster et al., 1997), and to assimilate into land surface models (Dong et al., 2007).

Kelly and Chang (2003) computed global maps of spatially varying coefficients a, obtained by re-calibrating the static algorithm using meteorological station data that are not time dependent. Foster et al. (2005) derived an alternate algorithm that made systematic error adjustments based on environmental factors including forest cover and snow morphology. Actually, they defined, for each snow class from Sturm et al. (1995), a correction parameter which changes each month. Nonetheless, this coefficient does not have interannual variability and within a class the snow grain size is supposed to be homogeneous. These algorithms, based on the Chang et al. (1987) initial formulation, allow spatially and even temporally varying coefficients but do not take into account the interannual snow crystal temporal evolution for each grid cells as do the dynamic and extended algorithms.

3.2. Dynamic algorithm

The dynamic algorithm (Josberger and Mognard, 2002; Mognard and Josberger, 2002) used in this study takes into account the internal snowpack properties, in particular the snow grain size temporal and spatial variability. The Thermal Gradient Index (TGI) represents the effect of the bulk temperature gradient through the snowpack and is a proxy for snow grain growth:

$$TGI = \int \frac{T_g - T_a}{D(t)} \quad (2)$$

where T_g is the ground temperature (K) at the interface between the ground and the snow and T_a is the air temperature (K) as defined in Section 2.3. Josberger and Mognard (2002) showed, using numerous in situ snow depth measurements in the Northern Great Plains of the USA, that a linear relationship exists between the spectral gradient SG and TGI:

$$SG = \alpha TGI + \beta. \quad (3)$$

Given the definition of TGI (Eq. (2)) and by differentiating the above equation, snow depth can be calculated as follows:

$$SD = \frac{\alpha (T_g - T_a)}{dSG/dt}. \quad (4)$$

Grippa et al. (2004) used the snow depth USAF/ETAC multi-year average (Foster and Davy, 1988) to determine the slope of the linear relation between SG and TGI, α, which has been set to a temporally and spatially constant value equal to 3.5. Yet, ETAC climatology, which ends in the 1980s, captures a snow cover regime quite different from the studied time period. Therefore, the amplitude of the retrieved snow depth fields might be biased compared to GSWP2. Subsequently, this issue can be solved.

In Eq. (4), the snow depth can only be computed when the spectral gradient dSG/dt is changing in time, i.e. when the snow grain size and/or depth is evolving at an appreciable rate. This happens early in winter season when a thin snowpack combined with cold air temperatures generates rapid crystal growth. Therefore snow depth is calculated using Eq. (4) at the beginning of the snow season and when dSG/dt decreases below a certain threshold (in this study 1 K/pentad, for more details see Grippa et al., 2004), the static algorithm is used (after the snowpack has been established), with the a coefficient (Eq. (1)) calculated to match the last snow depth estimate from the dynamic algorithm for each pixel. A spatially varying coefficient is then determined for each pixel from the snow depth value at the time of the transition between dynamic and static algorithm (the transition is usually reached in February depending on the location and the climatic conditions). Note that this spatially dependent coefficient differs from one winter year to the next. This combination of snow depths retrieved using Eq. (4) and the static algorithm, Eq. (1), presented above will be hereafter referred to as the dynamic algorithm.

3.3. Extended dynamic algorithm

Over some areas, snow depth cannot be computed because the spectral gradient does not change much in time throughout the entire snow season (dSG/dt is always below the threshold of 1 K/pentad). For these locations the spatially varying Chang algorithm is used with the *a* coefficient calculated as follows:

$$a = \frac{\text{SD}_{\text{ETAC}}(\text{January})}{(T_{b19H} - T_{b37H})(\text{January})} \tag{5}$$

where SD_{ETAC}(January) is the January snow depth from the ETAC multi-year average and $(T_{b19H} - T_{b37H})$ (January) is the average spectral gradient for January. This method allows the *a* coefficient to vary in space but not in time.

For the retrieval algorithms and the GSWP2 data, the monthly snow depth multi-year average was constructed by averaging the monthly fields from October 1987 to September 1995. To compare with the GSWP2 snow depth, the SSM/I-based multi-year averages have been mapped to a 1°×1° resolution grid using a polar cylindrical equidistant map projection. Finally, note that Greenland was not taken into account in the results presented herein (as it poses specific problems related to both the LSSs and the retrieval algorithms).

4. Results

4.1. Global validation

The GSWP2 January snow depth multi-year average is shown Fig. 3a, and the corresponding SSM/I derived January
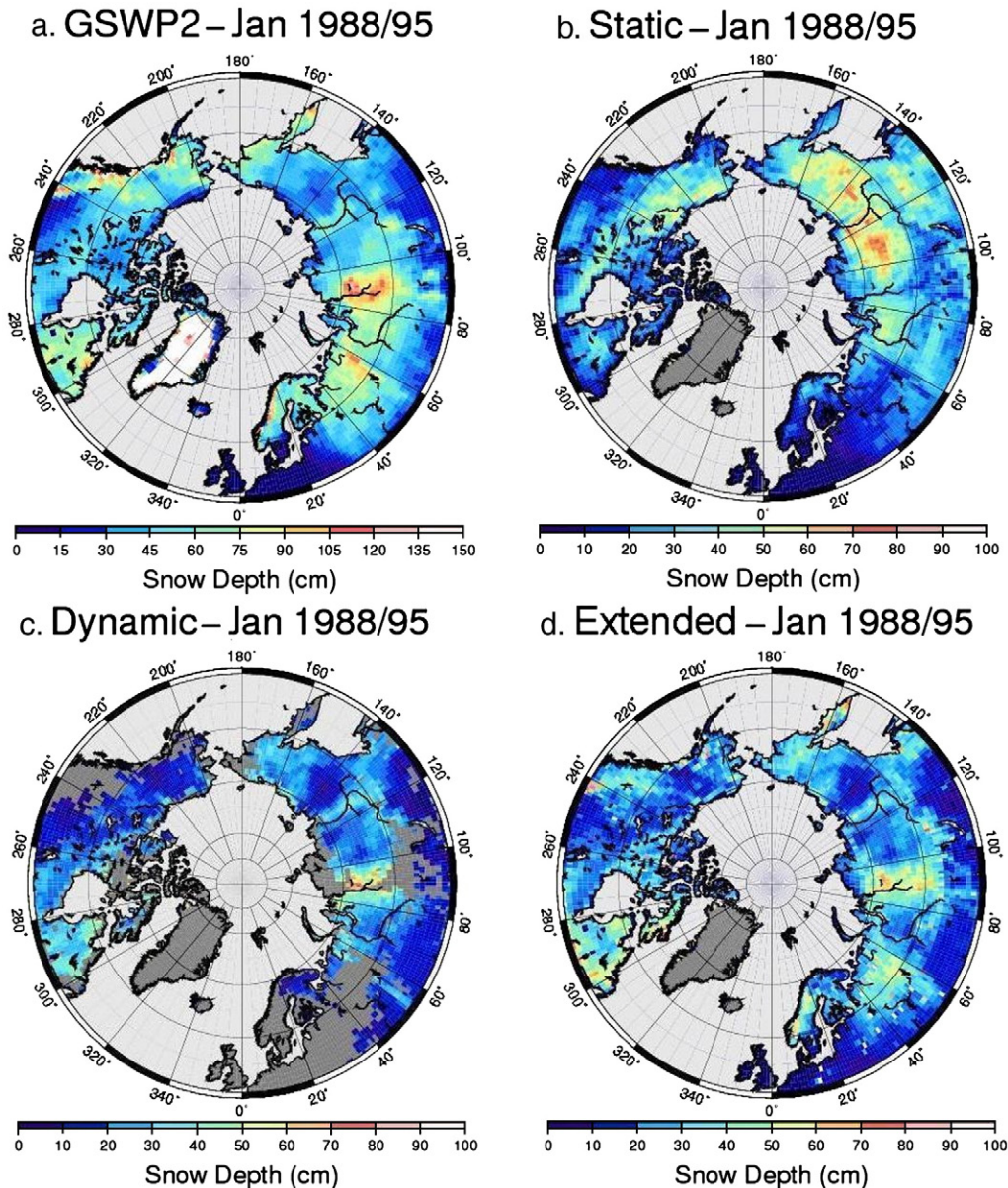

Fig. 3. Snow depth (cm) multi-year average for January (1988/1995) from GSWP2 (a), static algorithm (b), dynamic algorithm (c) and extended dynamic algorithm (d).

snow depth multi-year averages from the three retrieval algo-
rithms are shown in Fig. 3b, c and d. The three algorithms tend
to underestimate snow depth compared to GSWP2 (colour
scales are not the same in Fig. 3a and Fig. 3b, c, d). Some of the
discrepancy between GWSP2 and the SSM/I estimates could be
removed by tuning the a coefficient for the static algorithm
(Eq. (1)) and the α coefficient for the dynamic algorithm
(Eq. (4)). However, this has not been done because the purpose
of this study is to derive an average snowpack thickness using
currently available algorithms.

In Eurasia, the static algorithm (Fig. 3b) accumulates snow
over eastern Siberia (between 100°N and 180°N), whereas for
GSWP2 and for the dynamic and extended algorithms (Fig. 3a,
c, d) snow maxima are localized in western and central Siberia
(west of the Ural Mountains and Yenisey river basin, in
agreement with the location of maximum winter precipitation
patterns). Over North America, the static algorithm accumulates
snow along an east–west band located approximately at 60°N.
The GSWP2 data also shows snow in this region, but the
maximum snow accumulation is over the Rocky Mountains and
the eastern part of Canada in agreement with the location of
maximum winter precipitation patterns. The characteristic fea-
tures of snow accumulation regions obtained with the dynamic
and with the extended dynamic algorithms agree globally with
GSWP2. Over Eurasia, the better performance of the dynamic
algorithms over the static algorithm is particularly striking.
Over North America, the results of the visual comparison are
not as straightforward, but still the dynamic algorithm features
are in better agreement with the GSWP2 field than the static
algorithm. The regions of deepest snow pack obtained with the
static algorithm correspond to the regions where the coldest
winter air temperatures are recorded (Fig. 2d). The correlation
coefficient between the January NCEP air temperature field
(Fig. 2d) and the January static snow depth estimated field
(Fig. 3b) is −0.77, a much larger value then for any of the
correlation coefficient obtained with the GSWP2 snow depth
fields.

The dynamic algorithm (Fig. 3c) shows large regions where
snow depth cannot be computed. Some of these regions corre-
spond to mixed pixels along the coast line, to recurrent
occurrence of water in the snow pixel (succession of melt events
during winter season, especially west of the Ural Mountains), to
topography effects (for the Rocky Mountains and the Urals),
etc. For the period 1987/1995 snow depth cannot be computed
using only the dynamic algorithm for almost 34% of the study
domain, this issue is still under investigation. The extended
algorithm (Fig. 3d), that includes a priori information from the
ETAC snow multi-year average, shows accumulation in the
Rocky Mountains, the Ural Mountains and in the eastern part of
Alaska in agreement with GSWP2.

Monthly scatterplots, shown in Fig. 4, for the winter season
from October to March, compare the GSWP2 snow depth
estimates to the snow depths from both the static (first col-
umn) and the dynamic (second column) algorithms, only for
the pixels over which the dynamic algorithm is applied. In
this figure, each row corresponds to a winter month (from
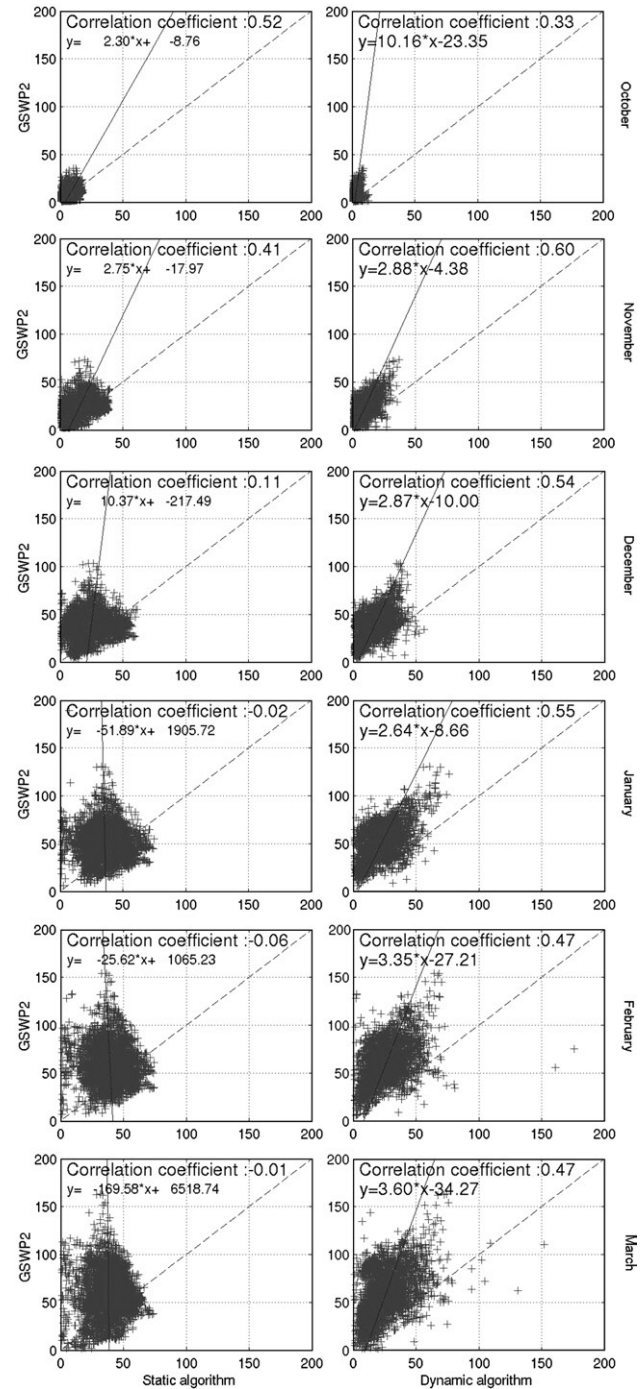October 1987/1994 to March 1988/1995). For each scatterplot,

Fig. 4. Scatter plots GSWP2 versus the static (first column) and the dynamic
algorithms (second column) with only the pixels over which the dynamic
algorithm is applied. For all the plots the y-axis corresponds to GSWP2 snow
depth (cm) and the x-axis corresponds to snow depth (cm) estimates using static
or dynamic algorithm. Each row corresponds to a month (from October to
March). The linear regression fits (solid lines, with its equation in the top left-
hand corner of each plot), the correlation coefficients and the line $y=x$ (dashed
lines) are also shown. Greenland has been eliminated.

the y-axis corresponds to snow depth from GSWP2 and the x-
axis corresponds to a retrieval algorithm. The coefficients of
correlation for the dynamic algorithm are of the same order of
magnitude, and for November to February are better, than the
correlation coefficient between the USAF/ETAC climatology

and GSWP2. After January, the correlation between dynamic algorithm and GSWP2 decreases slightly. Boone et al. (2006), link this decrease with two factors. First, ice layer formation, beginning of snow melt and reduction in snow grain size (arising from thermal gradients) impact the retrieval algorithms. Second, there is an increasing inter-model spread in time for GSWP2 snow depth multi-year average, because of increasing LSS differences during snow melt periods. Fig. 5 presents similar scatterplots, which correspond to GSWP2 snow depth (cm) versus the static (first column) and the extended dynamic (second column) algorithms for the whole high latitude regions (except Greenland). Apart from October, the dynamic and extended dynamic algorithms always have a better correlation coefficient with GSWP2 than the static algorithm, in agreement with the observations on the 2D plots (Fig. 3) in the preceding paragraph. There is no correlation between static algorithm and GSWP2 from December to March (correlation coefficient between 0.10 and −0.04). The poor performance of the dynamic algorithm in October can be explained by the high variability of the spectral gradient in the very beginning of the snow season, while the snowpack is not well established.

Fig. 5 shows that the plots GSWP2 versus extended algorithm have a larger amount of scattered points than the plots GSWP2 versus the dynamic algorithm. This could be explained by the fit of the spatially variable a coefficient in regions where the spectral gradient does not vary much in time.

Table 1 presents the correlation coefficients between GSWP2 and the three algorithms from October to March for the entire domain (latitude > 50°N), for Eurasia (latitude > 50°N and 0°-E < longitude < 191°E) and for North America (latitude > 50°N and 191°E < longitude < 360°E). For each correlation coefficient, a p-value has been calculated to estimate the statistical significance of the correlation. For the dynamic and the extended dynamic algorithm all the correlation coefficients are highly significant (all the p-values are under 0.001, except for the dynamic algorithm in October over North America, where the p-value is 0.05, which is a low value still significant). High p-values are obtained for the static algorithm after December, these values correspond to correlation coefficients close to zero. The comparison between Eurasia and North America reveals that the dynamic retrieval methods perform better over Eurasia than over North America. For example the correlation coefficient between GSWP2 and the dynamic algorithm in January over Eurasia is 0.65, whereas it decreases to 0.29 over North America. In Canada, many investigators have evaluated the accuracy of SSMI snow depth derived from an adjusted static algorithm tuned to the different land cover and obtained a good performance in the prairie and high latitude forest regions, but a poor performance in the high latitude tundra region (Derksen et al., 2003, 2004, 2005; De Seve et al., 1997).

4.2. Snow depth estimates over vegetation and lakes

To investigate the different behaviour of the SSMI derived monthly snow depth over Eurasia and North America, the vegetation and lake classifications described in Section 2.4.2 have been used. Tundra and taiga, the two predominant vege-
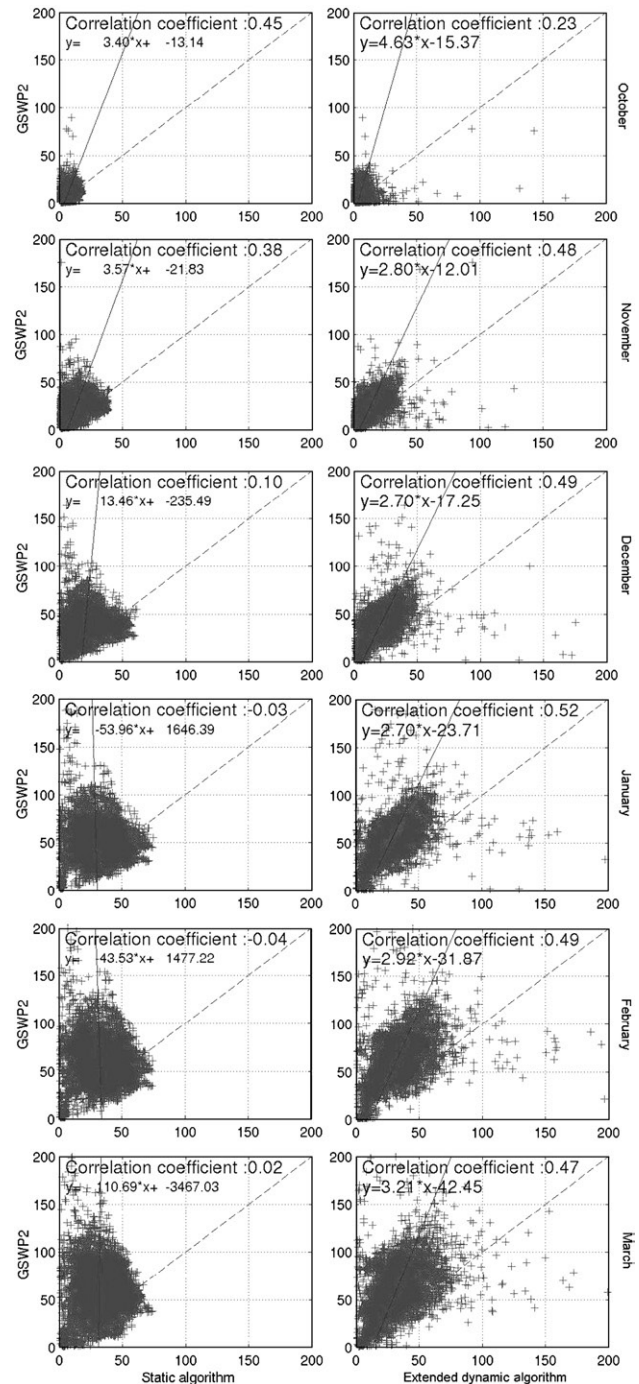

Fig. 5. Scatter plots GSWP2 snow depth (cm) versus the static (first column) and the extended dynamic algorithms (second column) snow depth (cm) for the whole high latitude regions (except Greenland). Each row corresponds to a month (from October to March). The linear regression fits (solid lines, with its equation in the top left-hand corner of each plot), the correlation coefficients and the line $y=x$ (dashed lines) are also shown.

tation types in the high latitude regions, as well as lake density modify brightness temperatures and therefore snow depth estimates (Duguay et al., 2005). Beside, GSWP2 models do not include lakes (only the land surface). So, in regions with high percentage of lakes, the differences between GSWP2 and SSM/I based algorithms data are expected to be quite significant. For the following analysis, only the snow estimates from the

Table 1
Correlation coefficients from October to March between the three algorithms and GSWP2, for three regions: the entire domain (latitude>50°N), Eurasia (latitude>50°N and 0°E<longitude<191°E) and North America (latitude>50°N and 191°E<longitude<360°E)

		Oct	Nov	Dec	Jan	Feb	Mar
Entire domain	Static	0.45	0.38	0.10	−0.03 (p=0.07)	−0.04 (p=0.01)	0.02 (p=0.26)
	Dynamic	0.33	0.60	0.54	0.55	0.47	0.47
	Extended	0.23	0.48	0.49	0.52	0.49	0.47
Eurasia	Static	0.62	0.50	0.18	0.01 (p=0.42)	−0.04 (p=0.01)	−0.03 (p=0.15)
	Dynamic	0.40	0.68	0.63	0.65	0.56	0.50
	Extended	0.29	0.53	0.57	0.61	0.59	0.52
North America	Static	0.27	0.27	0.01 (p=0.95)	−0.11	−0.02 (p=0.45)	0.16
	Dynamic	0.13 (p=0.05)	0.42	0.33	0.29	0.33	0.39
	Extended	0.20	0.46	0.35	0.33	0.33	0.36

For each correlation coefficient, p-value has been calculated to estimate the statistical significance of the correlation. On this table, only the p-values above 0.001 are shown in brackets below the correlation coefficient (correlation coefficients with p-values under 0.001 are highly significant).

dynamic algorithm have been used (not to be biased by the a priori information included into the extended algorithm).

Microwave radiation at 37 GHz is absorbed by vegetation (Chang et al., 1996). Yet, Hallikainen et al. (1988) found that emissivities for forests in Finland at 37 and 18 GHz are very similar with values of 0.9 to 0.92. Thus, the difference between brightness temperature at 37 and 18 GHz might not be very sensitive to the boreal forest. The impact of vegetation on the brightness temperature could influence the snow depth retrieval

algorithm, but this impact is very difficult to predict (compared to the static algorithm).

Fig. 6 shows the correlation coefficients between GSWP2 and the dynamic algorithm versus time (October to March) for the entire domain, for Eurasia and for North America as a function of snow classification type. For the entire domain (Fig. 6a), the correlation is globally better over taiga, whereas over tundra it is very close (and a bit lower) to the correlation over the global area. For Eurasia (Fig. 6b), the correlation over
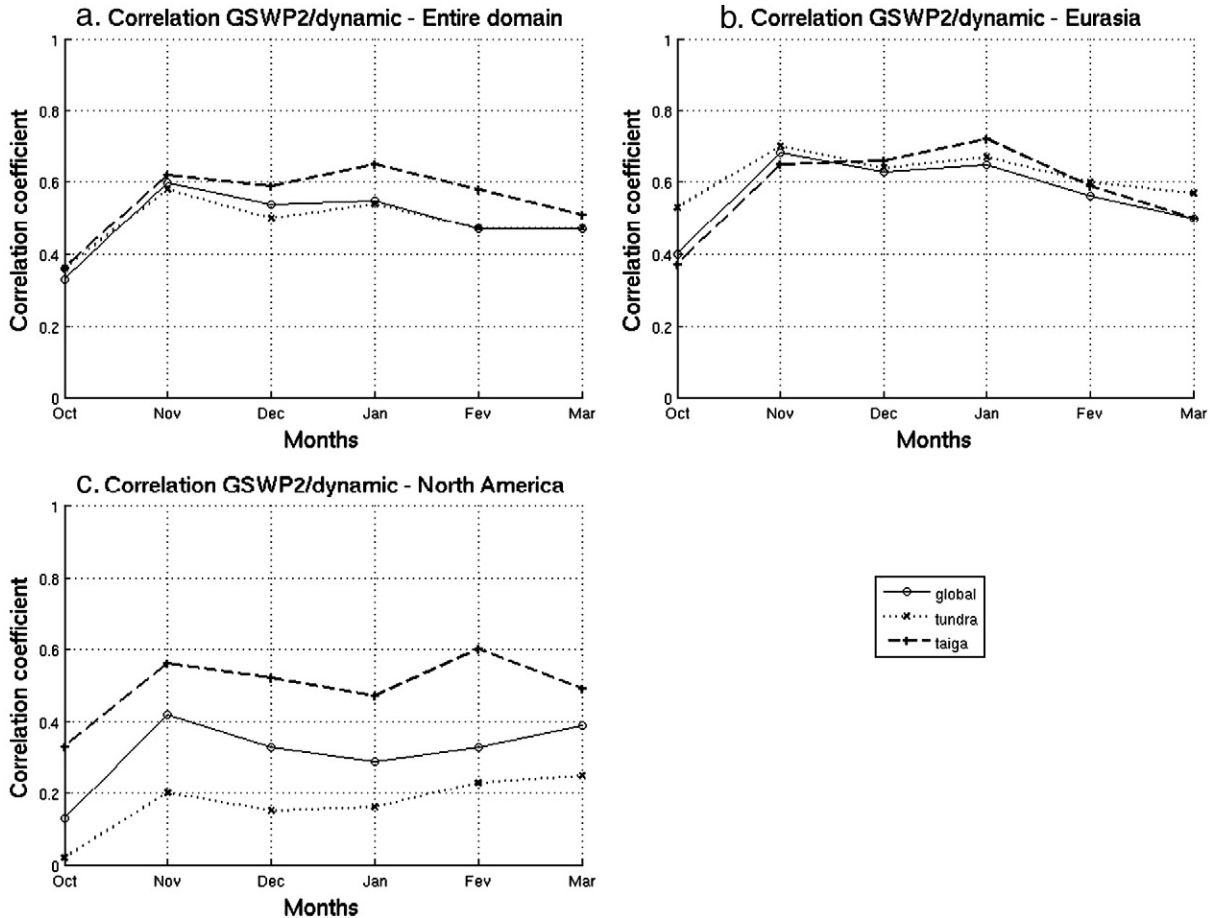

Fig. 6. Plots of correlation coefficients between GSWP2 and dynamic algorithm (y-axis) for each month from October to March (x-axis) for the entire domain (a), Eurasia (b) and North America (c). For each plot, correlations over the whole area (black solid line), over tundra (black dotted line) and over taiga (black dashed line) are shown. Classification between tundra and taiga comes from Liston and Sturm (1998) (Fig. 1b).

Table 2
Mean percentage of lakes for tundra, taiga and global area for the entire study domain, for Eurasia and for North America

	Entire domain			Eurasia			North America		
	Global	Tundra	Taiga	Global	Tundra	Taiga	Global	Tundra	Taiga
Mean % of lakes	6.8%	8.5%	4.4%	5.6%	7%	3.2%	9.1%	11%	7%

tundra and taiga is very similar. Thus, emissivity over Eurasia does not seem to be very sensitive to the distinction between tundra/taiga. For North America (Fig. 6c), the correlation is continuously higher over taiga than over tundra. This difference could be attributed to the relatively consistent distribution of snow properties in boreal forest, whereas, in the open tundra, snow depth could be highly variable and therefore very difficult to estimate because of wind redistribution (Derksen et al., 2005). So, we do observe a difference in the behaviour over tundra and taiga between the two continents: contrarily to Eurasia, North America seems to be significantly sensitive to vegetation type.

Emissivity from snow-covered lakes is different from terrestrial emissivity, yet the retrieval algorithms have been designed to work on land surfaces and do not take into account those differences. Indeed, contrarily to other land surfaces,

brightness temperature over lakes is higher at 37 than 19 GHz during both the ice-free and ice-covered periods (Duguay et al., 2005; Hall et al., 1981; Soko et al., 2003). The spectral gradient (difference between 19 and 37 GHz brightness temperature) will be smaller if there are lakes in the SSM/I pixel and can even be negative if the percentage of lakes is high enough. So both the static, dynamic and extended dynamic algorithms will be affected. Table 2 presents the mean percentage of lakes over the entire high latitude regions, over Eurasia, and over North America depending on the vegetation cover (tundra, taiga and the region as a whole). North America has almost twice as many lakes as Eurasia (mean percentage of lakes over North America is 9.1%, whereas it decreases to 5.6% over Eurasia) and for both continents the lake density is almost twice as dense in the tundra than in the taiga regions. The increased lake density could be responsible for the low correlation coefficients over North
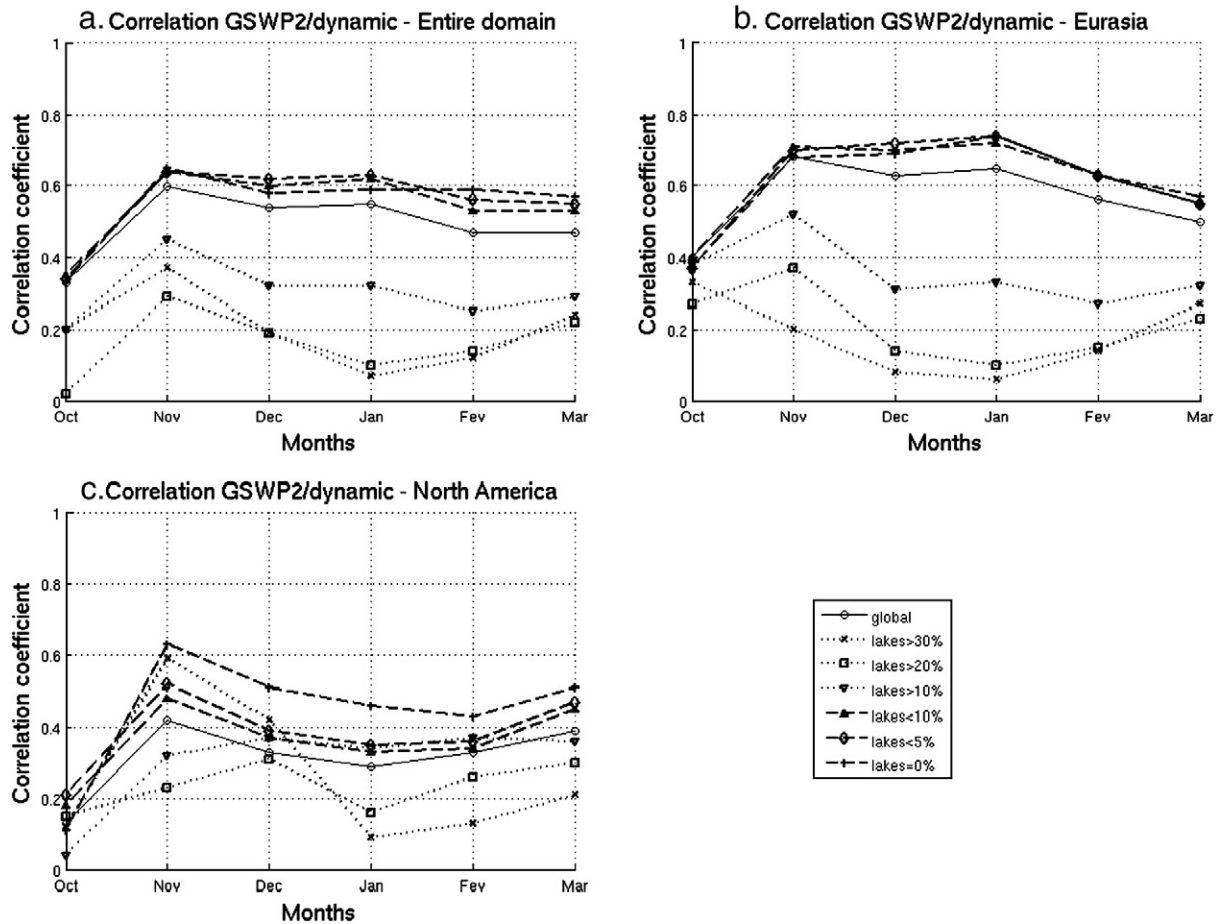

Fig. 7. Plots of correlation coefficients between GSWP2 and dynamic algorithm over regions with more than 30% (black dotted line with x markers), 20% (black dotted line with square markers), 10% (black dotted line with down triangle markers) of lakes and less than 10% (black dashed line with triangle markers), 5% (black dashed line with diamond markers) and 0% (black dashed line with + markers) of lakes and the whole area (black solid line) for the entire domain (a), Eurasia (b) and North America (c). The lake classification comes from IGBP (Fig. 1c).

America and may also explain the different behaviour over tundra and taiga between the two continents. Over North America the higher lake density may affect the microwave signal providing a significantly better snow depth retrieval in relatively lower lake density regions, the taiga region (mean lake density of 7%), than in the tundra (mean lake density of 11%), while over Eurasia the difference in lake density between tundra and taiga may be less relevant since it is in both cases lower than 7%. To better characterize the influence of lakes on the correlation between GSWP2 and the dynamic algorithm, the correlation coefficients have been plotted (Fig. 7) for different percentage of lakes (above 10%, 20%, 30% and below 10%, 5% and 0%) for the entire study domain (Fig. 7a), for Eurasia (Fig. 7b) and for North America (Fig. 7c). On this figure it appears clearly that correlation is better for lake sparse (less than 10%) than for lake rich (more than 30%) grid cells, except for November and December in North America.

5. Conclusion and perspectives

Global snow depth estimates over the Northern Hemisphere (above 50°N) have been derived from SSM/I data, using a static algorithm and a dynamic algorithm that takes into account the temporal and spatial variations of the snow grains size. The static algorithm, which is widely used, does not take into account the spatio-temporal variations of the snow pack and assumes a constant snow grain size. The snow depth fields estimated from the static algorithm do not correctly locates the regions of greater snow accumulation and do not significantly correlate to the GSWP2 snow depth fields (correlation coefficient −0.03 for January), but show a high degree of correlation with the NCEP air temperature fields (correlation coefficient −0.77 for January). The deepest satellite derived snow pack being located in regions with the lowest air temperatures. This justifies our hypothesis that one of the main driving factors for the microwave emissivity of the snow pack is the snow grain size determined by the thermal gradient in the snow pack. The dynamic algorithm correctly locates the regions of greater snow accumulation when compared to the GSWP2 output (correlation coefficient 0.55 for January, which can be considered good since there is much snow depth variability in a 25 by 25 km pixel due to wind effects, microscale topography,).

Since the dynamic algorithm is restricted to regions where the spectral gradient varies with time, an extended dynamic algorithm has been derived that allows to compute a global 2D satellite snow depth field and fills in the gaps where the dynamic algorithm cannot be applied. This extended dynamic algorithm also correlates well with the GSWP2 snow depth over the whole high latitude regions (with a correlation coefficient of 0.52 in January).

A comparison of the monthly satellite-derived snow depth multi-year averages over Eurasia and North America yields different behaviors. Over Eurasia the correlation with the models is better than over North America. The differences between Eurasia and North America could be explained by the differences in lake density, which is in North America almost twice as high as in Eurasia.

If the characteristic features of the GSWP2 snow depth fields have been correctly reproduced with the satellite derived fields, the amplitude of the signal has to be fine-tuned. There is a constant underestimation of the amplitude of the satellite fields compared to the GSWP2 fields (Figs. 4 and 5), which could be overcome by calibrating the α coefficient (Eq. (4)). We did not re-calibrate any of the models because the goal of this study was to determine if characteristic features of the multi-year averaged global snow depth in the high latitude regions can be derived from passive microwave satellite measurements, if the spatio-temporal evolution of the snowpack is correctly taken into account.

In the future, the new satellite derived snow depth fields can be used to study the interannual snowpack variability and better understand the hydrological cycle in the high latitude regions. A study over a test region, the Ob river basin in Siberia, showed that the interannual snowpack variability over the entire basin was correlated to the Ob in situ discharge measurements at the Ob estuary (Grippa et al., 2005a). A correlation between the snowpack variability and the summer vegetation activity in Siberia has been found, that could be explained by the protection provided by the snowpack from the cold Siberian temperatures (Grippa et al., 2005b). We plan to extend these regional analyses to the whole high latitude regions. Moreover, climate studies of the snow pack in the high latitude regions can also be performed, since the satellite passive microwave data set is continuous since 1979.

References

Armstrong, R. L., Knowles, K. W., Brodzik, M. J., & Hardman, M. A. (1994, updated 2003). DMSP SSM/I Pathfinder daily EASE-Grid brightness temperatures, 1987–1995. Boulder, CO, USA, National Snow and Ice Data Center (Digital media and CD-ROM).

Bamzai, A. S., & Shukla, J. (1999). Relation between Eurasian snow cover, snow depth and the Indian summer monsoon: An observational study. *Journal of Climate*, *12*, 3117−3132.

Belward, A. S., Estes, J. E., & Kline, K. D. (1999). The IGBP-DIS 1-Km Land-Cover Data Set DISCover: A project overview. *Photogrammetric Engineering and Remote Sensing*, *65*(9), 1013−1020.

Boone, A., Masson, V., Meyers, T., & Noilhan, J. (2000). The influence of the inclusion of soil freezing on simulations by a soil–vegetation–atmosphere transfer scheme. *Journal of Applied Meteorology*, *9*, 1544−1569.

Boone, A., Mognard, N., Decharme, B., Douville, H., Grippa, M., & Kerrigan, K. (2006). The impact of simulated soil temperatures on the estimation of snow depth over Siberia from SSM/I compared to a multi-model multi-year average. *Remote Sensing of Environment*, *101*, 482−494.

Cao, Z., Wang, M., Proctor, B., Strong, G., Stewart, R., Ritchie, H., et al. (2002). On the physical processes associated with the water budget and discharge over the Mackenzie basin during the 1994/95 water year. *Atmosphere-Ocean*, *40*(2), 125−143.

Chang, A. T. C., Foster, J. L., & Hall, D. K. (1987). Nimbus-7 SMMR derived global snow cover parameters. *Annals of Glaciology*, *9*, 39−44.

Chang, A. T. C., Foster, J. L., & Hall, D. K. (1990). Satellite sensor estimates of Northern Hemisphere snow volume. *International Journal of Remote Sensing*, *11*, 167−171.

Chang, A. T. C., Foster, J. L., & Hall, D. K. (1996). Effects of forest on the snow parameters derived from microwave measurements during the BOREAS Winter Field Campaign. *Hydrological processes*, *10*, 1565−1574.

Chang, A. T. C., Kelly, R. E. J., Josberger, E. G., Armstrong, R. L., Foster, J. L., & Mognard, N. M. (2005). Analysis of ground-measured and passive-microwave-derived snow depth variations in midwinter across the Northern Great Plains. *Journal of Hydrometeorology*, *6*, 20−33.

Derksen, C., Brown, R., & Walker, A. (2004). Merging conventional (1915–1992) and passive microwave (1978–2002) estimates of snow extent and water equivalent over central North America. *Journal of Hydrometeorology*, *5*(5), 850−861.

Derksen, C., Walker, A., & Goodison, B. (2003). A comparison of 18 winter seasons of in situ and passive microwave derived snow water equivalent estimates in Western Canada. *Remote Sensing of Environment*, *88*(3), 271−282.

Derksen, C., Walker, A., & Goodison, B. (2005). Evaluation of passive microwave snow water equivalent retrievals across the boreal forest/tundra transition of western Canada. *Remote Sensing of Environment*, *96*, 315−327.

De Seve, D., Bernier, M., Fortin, J. P., & Walker, A. (1997). Preliminary analysis of snow microwave radiometry using the SSM/I passive-microwave data: The case of La Grande River watershed (Quebec). *Annals of Glaciology*, *25*, 353−361.

Dirmeyer, P. A., Gao, X., Zhao, M., Guo, Z., Oki, T., & Hanasaki, N. (2006). GSWP-2: Multimodel analysis and implications for our perception of the land surface. *Bulletin of the American Meteorological Society*, *87*, 1381−1397.

Dong, J., Walker, J. P., Houser, P. R., & Sun, C. (2007). Scanning multichannel microwave radiometer snow water equivalent assimilation. *Journal of Geophysical Research*, *112*, D07108. doi:10.1029/2006JD007209

Duguay, C., Green, J., Derksen, C., English, M., Rees, A., Sturm, M., et al. (2005). Preliminary assessment of the impact of lakes on passive microwave snow retrieval algorithms in the Arctic. *62nd eastern snow conference, Waterloo, ON, Canada*.

Foster, J. L., Chang, A. T. C., & Hall, D. K. (1997). Comparison of snow mass estimates from a prototype passive microwave snow algorithm, a revised algorithm and snow depth multi-year average. *Remote Sensing of Environment*, *62*, 132−142.

Foster, D. J., & Davy, R. D. (1988). *Global Snow Depth Multi-Year Average, USAFETAC/TN-88/006*. Illinois: Scott Air Force Base. 48 pp.

Foster, J. L., Sun, C., Walker, J. P., Kelly, R. E. J., Chang, A. T. C., Dong, J., et al. (2005). Quantify the uncertainty in passive microwave snow water equivalent observations. *Remote Sensing of Environment*, *94*(2), 187−203.

Grippa, M., Kergoat, L., Le Toan, T., Mognard, N. M., Delbart, N., & L'Hermitte, J. (2005). The impact of snow depth and snowmelt on the vegetation variability over central Siberia. *Geophysical Research Letters*, *32*, L21412. doi:10.1029/2005GL024286

Grippa, M., Mognard, N. M., & Le Toan, T. (2005). Comparison between the interannual variability of snow parameters derived from SSM/I and the Ob river discharge. *Remote Sensing of Environment*, *98*, 35−44.

Grippa, M., Mognard, N. M., Le Toan, T., & Josberger, E. G. (2004). Siberia snow depth multi-year average derived from SSM/I data using a combined dynamic and static algorithm. *Remote Sensing of Environment*, *93*, 30−41.

Hall, A. (2004). The role of surface albedo feedback in climate. *Journal of Climate*, *17*, 1150−1568.

Hall, D., Foster, J., Chang, A. T. C., & Rango, A. (1981). Freshwater ice thickness observations using passive microwave sensors. *IEEE Transactions on Geoscience and Remote Sensing GE*, *19*(4), 189−193.

Hallikainen, M. T., Jolma, P. A., & Hyyppa, J. M. (1988). Satellite microwave radiometry of forest and surface types in Finland. *IEEE Transactions on Geoscience and Remote Sensing*, *26*, 622−628.

Josberger, E. G., & Mognard, N. M. (2002). A passive microwave snow depth algorithm with a proxy for snow metamorphism. *Hydrological Processes*, *16*(8), 1557−1568.

Kalnay, E., Kanamitsu, M., Kistler, R., Collins, W., Deaven, D., Gandin, L., et al. (1996). The NCEP/NCAR 40-year reanalysis project. *Bulletin of the American Meteorological Society*, *77*(3), 437−471.

Kanamitsu, M., Ebisuzaki, W., Woollen, J., & Yang, S. K. (2002). NCEP/DOE AMIP-II reanalysis (R-2). *Bulletin of the American Meteorological Society*, *83*, 1631−1643.

Kelly, R. E. J., & Chang, A. T. C. (2003, Mar 41). Development of a passive microwave global snow depth retrieval algorithm for Special Sensor Microwave Imagery (SSM/I) and Advanced Microwave Scanning Radiometer-EOS (AMSR-E) data. *Radio Science*, *38*(4), 1−11.

Liston, G. E., & Sturm, M. (1998). *Global Seasonal Snow Classification System*. Boulder, CO, USA: National Snow and Ice Data Center Digital media.

Mognard, N. M., & Josberger, E. G. (2002). Northern Great Plains 1996/97 seasonal evolution of snowpack parameters from satellite passive-microwave measurements. *Annals of Glaciology*, *34*, 15−23.

Noilhan, J., & Mahfouf, J. F. (1996). The ISBA land surface parameterization scheme. *Global and Planet Change*, *13*, 145−159.

Rango, A. (1997). Response of aerial snow cover to climate change in a snowmelt-runoff model. *Annals of Glaciology*, *25*, 232−236.

Rawlins, M. A., Willmott, C. J., Shiklomanov, A., Linder, E., Frolking, S., Lammers, R. B., et al. (2006). Evaluation of trends in derived snowfall and rainfall across Eurasia and linkages with discharge to the Arctic Ocean. *Geophysical Research Letters*, *33*, L07403. doi:10.1029/2005GL025231

Schlosser, C. A., Slater, A. G., Robock, A., Pitman, A. J., Vinnikov, K. Y., Henderson-Sellers, A., et al. (2000). Simulations of a boreal grassland hydrology at Valdai, Russia: PILPS phase 2(d). *Monthly Weather Review*, *128*, 301−321.

Soko, J., Pultz, T., & Walker, A. (2003). Passive and active airborne remote sensing of snow cover. *International Journal of Remote Sensing*, *24*(24), 5327−5344.

Sturm, M., & Benson, C. S. (1997). Vapor transport, grain growth and depth-hoar development in the subarctic snow. *Journal of Glaciology*, *43*(143), 42−59.

Sturm, M., Holmgren, J., & Liston, G. E. (1995). A seasonal snow cover classification system for local to regional applications. *Journal of Climate*, *8*, 1261−1283.

Tsang, L., Chen, C. T., Chang, A. T. C., Guo, J., & Ding, K. H. (2000). Dense media radiative transfer theory based on quasicrystalline approximation with application to passive microwave remote sensing of new snow. *Radio Science*, *35*(3), 731−749.

Wulder, M. A., Nelson, T. A., Derksen, C., & Seemann, D. (2007). Snow cover variability across central Canada (1978–2002) derived from satellite passive microwave data. *Climatic Change*, *82*, 113−130. doi:10.1007/s10584-006-9148-9